

Influence of composite admixtures on the freezing resistance and pore structure characteristics of cemented sand and gravel

 L. Guo^{abc},  W. Wang^a,  L. Zhong^{abc}✉,  L. Guo^{abc},  L. Wang^{abc},  M. Wang^a,  Y. Guo^a,  P. Chen^a

a. School of Water Conservancy, North China University of Water Resources and Electric Power, (Zhengzhou, China)

b. Henan Water Valley Research Institute, (Zhengzhou, China)

c. Henan Key Laboratory of Water Environment Simulation and Treatment, (Zhengzhou, China)

✉: wwk9702@126.com

Received 29 October 2021

Accepted 3 April 2022

Available on line 28 June 2022

ABSTRACT: CSG shows low freezing resistance due to its poor cementing properties, and adding admixtures is the main method to improve its freezing resistance. In this paper, experiments were designed based on the Taguchi method and on the freezing resistance and pore structure characteristics of CSG after adding admixtures. After 20 freeze-thaw cycles, the results showed that both the compressive strength and dynamic elastic modulus of CSG decreased. The area occupancy of more harmful pores (>200 nm) in the NMR test increased, and the fractal dimension of the pore structure in the SEM images also increased. Based on the above indicators, it was concluded that L9 (sodium dodecyl sulfate, graphene oxide, nanosilica powder, and water-reducing agent) has the best freezing resistance. Experiments were conducted on L9 to verify that L9 can significantly improve the freezing resistance of CSG materials under different water-binder ratios, sand ratios, and cement dosages.

KEY WORDS: Cemented sand and gravel; Freezing resistance; Fractal dimension; Pore structure; Composite admixtures.

Citation/Citar como: Guo, L.; Wang, W.; Zhong, L.; Guo, L.; Wang, L.; Wang, M.; Guo, Y.; Chen, P. (2022) Influence of composite admixtures on the freezing resistance and pore structure characteristics of cemented sand and gravel. *Mater. Construcc.* 72 [347], e290. <https://doi.org/10.3989/mc.2022.16021>.

RESUMEN: *Influencia de los aditivos compuestos en la resistencia a la congelación y las características de la estructura de los poros de grava y arena cementada.* La CSG presenta una baja resistencia al congelamiento debido a sus pobres propiedades cementantes. Añadir aditivos es el método principal para mejorarla. Para este artículo, se diseñaron experimentos basados en el método Taguchi y en las características de resistencia al congelamiento y la estructura de los poros de CSG después de añadir aditivos. Tras 20 ciclos hielo-deshielo, disminuyeron la resistencia a compresión y el módulo de elasticidad dinámico de la CSG. La superficie ocupada por los poros más dañinos (>200 nm) aumentaba según los resultados de RMN, e igualmente aumentaba la dimensión fractal de su estructura en las imágenes SEM. Atendiendo a los indicadores anteriores, se concluyó que la muestra L9 (laurilsulfato sódico, óxido de grafeno, polvo de nanosilice y agente reductor de agua) tiene la mejor resistencia. Se ejecutaron experimentos con L9 para verificar que puede mejorar significativamente la resistencia al congelamiento de los materiales de CSG bajo diferentes dosis de cemento, proporciones de agua/aglutinante y de arena.

PALABRAS CLAVE: Grava y arena cementada; Resistencia al congelamiento; Dimensión fractal; Estructura de poros; Aditivos compuestos.

Copyright: ©2022 CSIC. This is an open-access article distributed under the terms of the Creative Commons Attribution 4.0 International (CC BY 4.0) License.

1. INTRODUCTION

Cemented sand and gravel (CSG) is a new kind of environmentally material for dam construction. It is made by simply mixing a few cementing materials into the riverbed sand and gravel, excavated waste materials, or other rock-based materials that are easy to obtain near a dam site, making it cost-effective and environmentally (1-4). L. Guo *et al.* (5) introduced fractal theory to study the effect of aggregate properties on CSG properties, quantifying aggregate gradation and shape. The results shown that the closer the aggregate gradation to the standard gradation, the better the performance of the CSG; as the proportion of polygonal aggregates increased, the worse the performance of the CSG. However, due to the small amount of cement, the CSG also reflects the shortcomings of its own material, its compressive strength is small, and its frost resistance is poor. As far as cement-based materials are concerned, an appropriate amount of additives can improve their mechanical properties and durability. Sanri-Karapinar, I., *et al.* (6) used κ -carrageenan/PVA/eggshell nanostructures as a novel biodegradable and homogeneous nanostructure in cement compositions, which improved the compressive strength and flexural strength of cement-based materials. Yildirim, M., & Derun, E. (7) studied the compressive and flexural strengths, thermal properties and pore structure of two types of boron waste and different amounts of CuO nanoparticles-modified mortars. It was observed that nano-CuO addition in the range 2%–2.5% can improve mechanical properties. Hernández, EF, *et al.* (8) investigated the mechanical performance and durability of concrete with water/cement (w/c) ratios of 0.30 and 0.60 containing cactus mucilage and brown marine seaweed extract solutions. It was found that when the water cement ratio was 0.60, the compressive strength of concrete after 120 days increased by 20% compared with the control group. Silva, Bruna, *et al.* (9) investigated the freeze-thaw resistance of lime mortar with different types of admixtures (water reducers, viscosity modifiers, air-entraining agents, and water repellents). Results showed that the water-reducer (superplasticizer) based on polynaphthalene sulfonate and the water-repellent based on silicone resin were the admixtures that more significantly improved the resistance to freeze-thaw, followed by the air-entrainers based on sodium dodecyl sulfate and sodium alfa-olefin sulfonate. Behfarnia, K., & Salemi, N. (10) investigated the frost resistance and mechanical properties of concrete containing nano-silica and nano-alumina. The results showed that the frost resistance of concrete containing nano- Al_2O_3 was better than that of concrete containing the same amount of nano- SiO_2 . However, its compressive strength is lower than that of concrete containing the same amount of nano- SiO_2 . As a special cement-based materials, CSG can also improve its freeze-thaw resistance durability by adding appropriate amount of admixtures. In cold regions, freeze-thaw

damage is the main factor causing the failure of a CSG dam and greatly shortens the service life of the dam. Some experts believe that there is a strong correlation between indoor freeze-thaw tests and actual field engineering (11-13). Therefore, it is of particular importance to study how to improve the freezing resistance of CSG materials through laboratory experiments.

At present, there are few studies on improving the freezing resistance of CSG materials, as the main focus has been mixing the proper amount of cementing materials and the enhancing effect of a single admixture. Xu Long (14) studied the effects of the type and content of traditional sodium alpha-olefin sulfonate (AOS) air-entraining agent and lightweight ceramsite (clay sand, polystyrene particles, and rubber powder of different fineness) on the freezing resistance of CSG, and the results showed that the freezing resistance of CSG increases with the increase in the content of AOS air-entraining agent, and light ceramsite can improve the freezing resistance of CSG to a certain extent. Feng Wei and Jia Jinsheng *et al.* (15) studied the freezing resistance of CSG under the action of air freezing and water freezing after the addition of admixtures (water-reducing agent and air-entraining agent). For CSG with an additive, the impermeability level at 180 d can reach W12, and it was destroyed in over than 75 freezing-thawing cycles in water but not destroyed in over 350 cycles in air. Matsumura K *et al.* (16) introduced air freezing and water freezing in CSG freeze-thaw tests, and their results showed that the freezing resistance of CSG with air freezing is approximately 10 times that of water freezing. Chen S, Zheng Y *et al.* (17) established a CSG freeze-thaw damage evolution model, which can predict the freezing resistance of CSG. G. Jin *et al.* (18) studied the influence of cement content on the strength and durability of CSG through freeze-thaw tests. As a result, the strength and durability of CSG are reliable when the amount of cement is over 0.8 kN/m^3 . Yeon K S *et al.* (19) studied the freeze-thaw resistance of CSG per unit of cement content. The above research shows that adding a single admixture can indeed improve the freezing resistance of CSG, but the effect is limited. Therefore, this paper investigates the effect of mixing multiple admixtures on the freezing resistance and pore structure of CSG and seeks a compound admixture to improve the freezing resistance of CSG.

2. RAW MATERIALS AND EXPERIMENTAL METHODS

2.1 Experimental materials

In this experiment, P•O 42.5 Portland cement produced by Henan Tianrui Co., Ltd. was selected, and its technical indicators are detailed in Table 1. The fly ash used was Class I ash from the Yulian Power

Plant, and its technical performance meets the relevant requirements in GB/T1596-2017 fly ash used for cement and concrete; see Table 2 for details. The fine aggregate was produced by Tanghe County Xinmiao Sand Co., Ltd., with a fineness modulus of 2.94 and a bulk density of 1,625.0 kg/m³. The coarse aggregate used was natural pebbles dug out from a riverbed. Containing a large amount of mud, the pebbles were cleaned before the experiment, and those with particle sizes of 5-20 mm and 20-40 mm were screened. The mixing water was tap water from the laboratory.

Five kinds of admixtures were selected, namely sodium dodecyl sulfate, triterpenoid saponins, graphene oxide, nano silicon powder, and polycarboxylate superplasticizer. Their characteristics are shown in Table 3.

2.2 Mixing ratio

The basic mixing ratio of CSG is shown in Table 4, where the water–binder ratio is 1.0 and the sand ratio is 0.3.

Due to multiple admixtures, this experiment was designed using the Taguchi method (20, 21). Five factors were selected, namely sodium dodecyl sulfate (A), triterpenoid saponins (B), graphene oxide (C), nano silicon powder (D) and polycarboxylate superplasticizer (E), and four levels were selected for each factor to design the L16 (4⁵) orthogonal arrays, as shown in Tables 5 and 6, where L1 is the blank group.

TABLE 1. Mechanical properties of cement.

Specific surface area/(m ² ·kg ⁻¹)	Density/(kg·m ⁻³)	Setting time/min		Compressive strength/MPa		Flexural strength/MPa	
		Initial	Final	3 days	28 days	3 days	28 days
348.7	3035	176	244	25.9	49.6	5.6	8.6

TABLE 2. Chemical composition of cement and fly ash (%).

Materials	SiO ₂	Al ₂ O ₃	Fe ₂ O ₃	CaO	K ₂ O	TiO ₂	MgO	Na ₂ O	SO ₃	P ₂ O ₅
Cement	24.13	9.25	3.65	51.27	0.79	-	4.98	1.95	2.46	-
Fly Ash	53.97	31.15	4.16	4.01	2.04	1.13	1.01	0.89	0.73	0.67

TABLE 3. Admixture performance.

Sodium dodecyl sulfate	Molecular formula		Active matter content		Form		Color
	CH ₃ (CH ₂) ₁₁ OSO ₃ Na		≥86%		Needle-like micronucleus		White or light yellow
Triterpenoid saponins	Gas content (%)		Active matter content		Form		Color
	5.5		≥50%		powder		brown
Graphene oxide	Diameter	Stripping rate	carbon content	oxygen content	sulphur content	Form	Color
	1-10μm	>95%	<48%	>50%	<2%	powder	tan
Nano silicon powder	average size	purity (%)	specific surface area (m ² /g)	volume density (g/m ³)	density (g/m ³)	crystal form	Color
	20nm	99.9	240	0.06	2.2-2.6	irregular	White
Polycarboxylate Superplasticizer	Gas content (%)			water reduction (%)			pH
	4.4			15			4.56

TABLE 4. Mixing ratio of materials.

Material varieties	Cement	Fly ash	Water	Sand	stones	
					20-40mm	5-20mm
Dosage/kg·m ⁻³	70	20	90	636	890.4	593.6

TABLE 5. Taguchi test factors - level table.

Level	Factor	A	B	C	D	E
1		0	0	0	0	0
2		0.004%	0.005%	0.02%	0.50%	0.40%
3		0.008%	0.01%	0.04%	1.00%	0.80%
4		0.012%	0.02%	0.06%	2.00%	1.20%

Note: The actual dosage of admixture is the percentage of cementitious material.

TABLE 6. Admixture orthogonal group design.

Sample	A	B	C	D	E
L1	1	1	1	1	1
L2	1	2	2	2	2
L3	1	3	3	3	3
L4	1	4	4	4	4
L5	2	1	2	3	4
L6	2	2	1	4	3
L7	2	3	4	1	2
L8	2	4	3	2	1
L9	3	1	3	4	2
L10	3	2	4	3	1
L11	3	3	1	2	4
L12	3	4	2	1	3
L13	4	1	4	2	3
L14	4	2	3	1	4
L15	4	3	2	4	1
L16	4	4	1	3	2

2.3 Preparation and curing of the test pieces

The specimens were 100 mm × 100 mm × 100 mm for the uniaxial compression test and 100 mm × 100 mm × 400 mm for freeze–thaw test. First, add the weighed cementitious materials and aggregate into HJW100 mixer in sequence, and stir for 1min. Next, add the mixture of compound admixture and water to the blender and stir for 2min. Finally, the mixture is filled into steel moulds of corresponding size. Put the mold with the material on the vibrating table and vibrate for 60s. After pouring, the specimens were placed indoors for 24 hours and then demolded. The demolded specimens were transferred to a standard curing room (temperature 20±2°C, humidity 95%) for curing for 28 days.

2.4 Experimental methods

The experiment was performed in accordance with the standard for test methods of concrete physical and

mechanical properties (GB/T50081-2019) (22), test code for hydraulic roller compacted concrete (DL/T 5433-2009) (23), standard for test methods of long-term performance and durability of ordinary concrete (GB/T 50082-2009) (24) and other standards.

2.4.1 Compressive strength test

The compressive strength test adopted a WAW-1000 electrohydraulic servo universal testing machine. The specimens was a 100 mm×100 mm×100 mm specimens before and after freezing and thawing. During the test, the specimens was continuously and uniformly loaded at a speed of 5 kN/s until it fractured, and the peak failure load P was recorded to calculate the compressive strength.

2.4.2 Freezing resistance test

The freeze–thaw test was performed with three specimens as a group. First, a 100 mm × 100 mm ×

400 mm specimens that had been cured to 24 days of age was soaked in water at $20\text{ }^{\circ}\text{C} \pm 3\text{ }^{\circ}\text{C}$ for four days. Second, the specimens were removed, and the surface moisture was wiped off. We weighed the initial mass m_0 and the initial transverse fundamental frequency f_0 of the specimens, put the specimens into the test box, and tap water was added until the level was 20 mm higher than the top surface of the specimens. Finally, the test box containing the specimens was put into a freeze–thaw box containing a freeze–thaw solution with a temperature of $-25\text{ }^{\circ}\text{C}$ to $20\text{ }^{\circ}\text{C}$, and the parameters of the freeze–thaw machine were set: the cycle lasts 4.0 h, the cooling lasts 2.5 h, and the heating lasts 1.5 h. After 20 freeze–thaw cycles, we measured the mass m_{20} and the transverse fundamental frequency f_{20} of the specimens again, and calculated the relative dynamic elastic modulus and mass loss rate through Equation [1] and [2] to characterize the freezing resistance of the CSG.

The relative dynamic elastic modulus was calculated using the following formula:

$$P = E_{dn} / E_{d0} = Cmf_n^2 / Cmf_0^2 = f_n^2 / f_0^2 \times 100 \quad [1]$$

Where P is the relative dynamic elastic modulus (%) of the CSG specimens after the N -th freeze–thaw cycle; E_{dn} is the dynamic elastic modulus (MPa) of the CSG specimens after the N -th freeze–thaw cycle; E_{d0} is the dynamic elastic modulus (MPa) of the CSG specimens before the freeze–thaw cycle test; C is the shape calculation parameter (kg/m^2); m is the mass of the specimen (kg); f_n is the transverse fundamental frequency (Hz) of the CSG specimens after the N -th freeze–thaw cycle; f_0 is the initial transverse fundamental frequency (Hz) of the CSG specimens before the freeze–thaw cycle test.

The mass loss rate was calculated using the following Equation [2]:

$$\Delta M_n = (M_0 - M_n) / M_0 \times 100 \quad [2]$$

Where ΔM is the mass loss rate (%) of the specimens after the N -th freeze–thaw cycle; W_0 is the mass (g) of the specimens before the freeze–thaw cycle test; and W_n is the mass (g) of the specimens after the N -th freeze–thaw cycle.

2.4.3 Scanning electron microscopy test

A broken specimens from compression tests was randomly selected for scanning electron microscopy (SEM) examination. Before the SEM test, the sample was polished and ground to a size of approximately 10 mm and fixed on the sample base with conductive adhesive for metal spraying. The spraying thickness was 200–300 Å. During the test, a Quanta-650 Environmental Scanning Electron Microscope (ESEM) and an Apollo-X Spectrometer was used. working conditions: Test in BSE

mode, the acceleration voltage was 25kV, the SEM scanning time was 45 seconds, and the EDS scanning time was 3~5min. The sample magnification was 500~5000×.

2.4.4 Pore structure analysis

2.4.4.1 Porosity test

A MesoMR12-060H-I nuclear magnetic resonance device was used in the test. First, the specimen with an age of 28 days for 24 hours vacuum saturation, and then the specimen was put into the coil of the nuclear magnetic resonance instrument. NMR relaxation measurements were carried out by a nuclear magnetic resonance analysis system. After the Carr–Purcell–Meiboom–Gill (CPMG) sequence attenuation signal data were collected, the data inversion was performed to obtain the T2 spectrogram which was then converted into a pore size distribution diagram. The pore size was measured between 50 nm and 200 μm .

2.4.4.2 Pore structure characterization based on SEM images

With reference to the technology adopted by Liu et al (25) pore and crack analysis system (PCAS) software was used to obtain the pore binary characteristics. The threshold segmentation method was used to binarize the electron microscope images, and the different gray values of pores and hydration products in the images were used as the basis for distinguishing. Select an SEM image and put it into the software to convert it into a binary image by setting an appropriate threshold. The first step is to set a larger threshold. At this time, many elements that are originally hydration products are identified as pores and appear white. And then reduce the threshold appropriately until the fine hydration products in the pores are just identified, which is a more appropriate threshold at this time. The user determines the threshold for the relationship between pores and hydration products. The microscopic image is usually processed three times in different periods to reduce subjective errors. When the average value of the difference does not exceed 2 degrees, the average value of the three selected thresholds is obtained, which is the final selected threshold. For each series of experimental samples, at least 3 SEM images were recorded, and the average value was taken as the value of digital image quantitative processing. In this study, the SEM image with a magnification of 1000 times was selected as the original image processed by PCAS. Pores of 0~25 μm were collected. The distribution characteristics of irregular pores were quantified by fractal dimension (26). An example of pore structure feature extraction is shown in Figure 1.

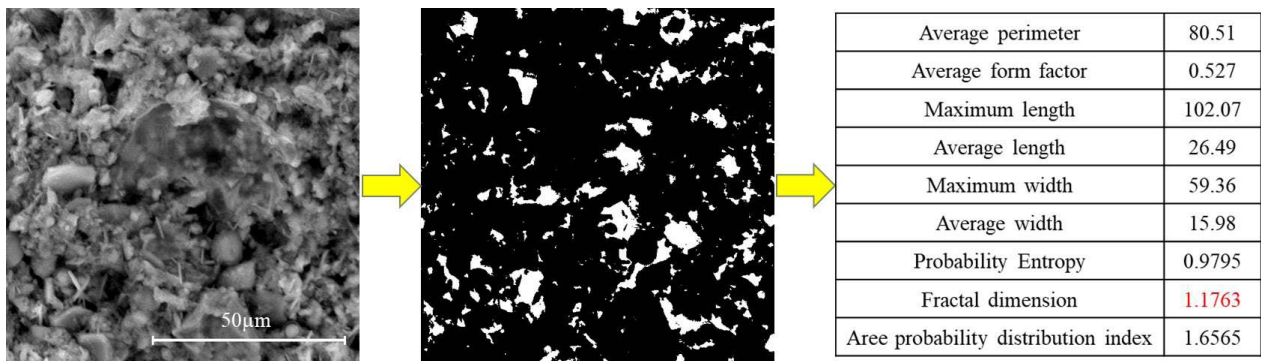


FIGURE 1. Pore structure test.

3. RESULTS AND ANALYSIS

3.1 The influence of composite admixtures on the freezing resistance of CSG

3.1.1 Compressive strength

The compressive strength of the CSG before and after freezing and thawing is shown in Figure 2. Compared with the blank group (L1), the pre-freezing compressive strength of the CSG test pieces after being mixed with composite admixtures all decreased to varying degrees. The reasons for this phenomenon are as follows: (1) After the air-entraining agent was introduced, a large number of tiny, closed and uniformly distributed polar bubbles were formed inside the CSG test pieces, which were beneficial to the workability of the mixtures, but reduced the effective compressive area, resulting in different degrees of strength loss of the test pieces mixed with admixtures; (2) both the water reducing agent and the air-entraining agent can reduce water (27); thus, in this study, the actual water–binder ratio was large and interfered with the hardening process of the CSG test pieces. Finally, microcracks appeared on the test pieces, reducing their strength. In accordance with the design requirements of CSG compressive strength specified in the Technical Guideline for Cemented Granular Material Dams (28) (SL 678-2014), the strength loss rate should be less than 20%; that is, the design strength should reach 8 MPa. Figure 2 shows that the test groups L2, L3, L6, L9, L10, and L13 met the compressive strength requirements.

To clarify the influence of composite admixtures on the mechanical properties of CSG, the strength loss rates of the L2, L3, L6, L9, L10, and L13 groups that met the requirements of the specification were analyzed and calculated, as shown in Figure 3. The compressive strength loss rates before and after freezing and thawing were all lower than that of the blank group (22.50%), indicating that adding composite admixtures is beneficial to improving the freezing resistance durability of CSG. Figure 2 and 3 show that, when the

range of strength loss is met, the strength loss rate of L9 before and after freezing and thawing is the smallest, at only 0.92%, and its admixtures include 0.008% sodium dodecyl sulfate, 0.04% graphene oxide, 2.0% nano silicon powder, and 0.40% water reducing agent.

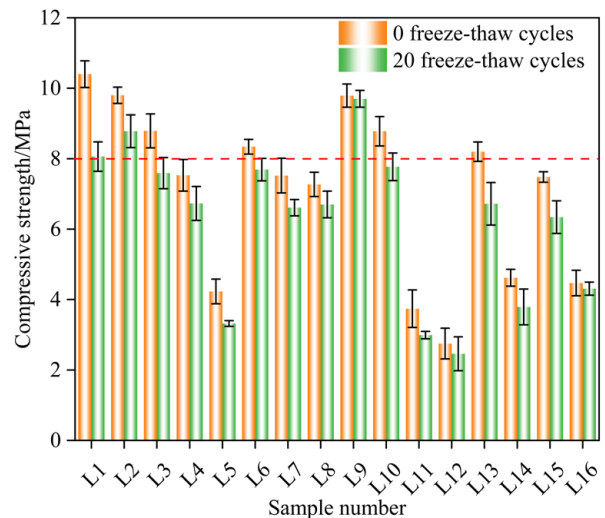


FIGURE 2. Compressive strength of CSG.

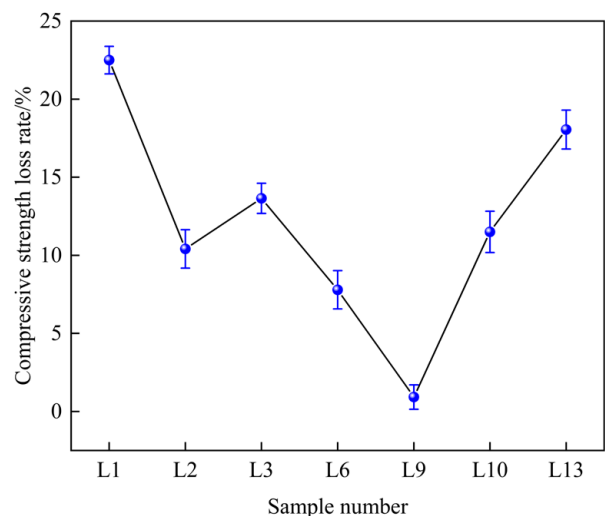


FIGURE 3. Compressive strength loss rate.

3.1.2 Relative dynamic elastic modulus

The dynamic elastic modulus is a main indicator that reflects the internal structural performance of a material. For freezing resistance, the smaller the relative dynamic elastic modulus is, the more obvious the effect of freeze–thaw damage is (29). Similarly, for CSG, the relative dynamic elastic modulus can also characterize its freeze–thaw damage (30). Figure 4 shows changes in the relative dynamic elastic modulus of CSG with different admixtures. Compared with the blank Group L1 (62%), the relative dynamic modulus of CSG with admixtures in the test groups was significantly higher. The relative dynamic elastic moduli of L5, L7, L8, L12, and L13 all exceed 80%, indicating that they have better freezing resistance. However as seen in Figure 2, after 20 freeze–thaw cycles, none of them meets the design standard of compressive strength. Therefore, the relative dynamic elastic modulus cannot be selected as the only indicator to evaluate the freezing resistance of CSG, and other indicators need to be considered together (31–33).

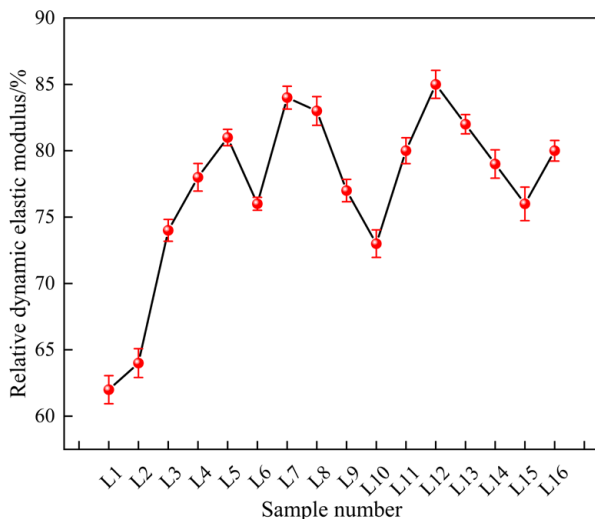


FIGURE 4. Relative dynamic elastic modulus of CSG.

3.2 The influence of composite admixtures on the pore structure of CSG

3.2.1 NMR pore analysis

NMR technology has been widely used in the study of microscopic pore structures and damage mechanisms of rocks and concrete (34–36). Figure 5 summarizes the pore size distribution of the test pieces before and after freezing and thawing obtained by NMR. Academician Wu Zhongwei (37) classified pores of 0–0.02 μm into harmless pores, pores of 0.02–0.05 μm into less harmful pores, pores of 0.05–0.2 μm into harmful pores, and pores above 0.2 μm into more harmful pores. Figure 5

shows that the harmless pores, less harmful pores and harmful pores are concentrated in the first peak, and the more harmful pores are mainly in the second and third peaks. The pore size distribution curves of the L5, L11, L12, L13, L14, and L16 groups before and after freezing and thawing have relatively larger changes. After freezing and thawing, the first peak is approximately 0.025%, and the second and third peaks increase. For example, the second peak value of the L13 group before freezing was 0.006%, and the pore diameter was 1.17 μm ; after freezing, the second peak value rose to 0.0084%, and the pore size increased to 1.45 μm . The pore size distribution curves of L9 and the rest of the test groups in the first peak are basically the same and show little change before and after freezing and thawing, approximately 0.02%, and the changes of the second and third peaks are different, but both move to the right. For example, the second peak pore size of the test pieces in the L9 group before freezing was 1.35 μm ; the corresponding value after freezing was 1.45 μm .

The area occupancy of more harmful pores was calculated according to the pore size distribution diagram, as shown in Figure 6. After 20 freeze–thaw cycles, the area occupancy of more harmful pores of CSG increases to varying degrees, and especially in the L5, L11, L12, L13, and L14 groups, it increased by 48.93%, 49.87%, 30.45%, 36.03%, and 75.50%, respectively, which verifies the above analysis. The reason for such phenomena is that at the beginning of freezing and thawing, harmless, less harmful and harmful pores with small sizes are internally filled with pore water, which may generate a frost heaving force due to the differential pressure inside and outside during freezing and thawing. In such cases, the pore wall is damaged, the pore size increases, and many pores are changed to more harmful pores. More harmful pores themselves are large in size and will become even larger under the frost heaving force until the test pieces undergo freeze–thaw damage.

The CSG test pieces experienced a gradually changing damage process under the action of water freeze–thaw cycles, and the damage pattern of its pore structure is shown in Figure 7. With the increase of the number in freeze–thaw cycles, the pore water in the test piece undergoes repeated volume expansion, resulting in the gradual enlargement of the pores and the increase in the degree of irregularity until penetrating cracks develop. The number of damage points inside the specimen increases, which leads to a decrease in its compressive strength.

3.2.2 Fractal characteristics of pore structure in SEM images

CSG images obtained before and after freezing and thawing in the SEM test are shown in Figure 8. Due to the large number of test groups, only partial SEM

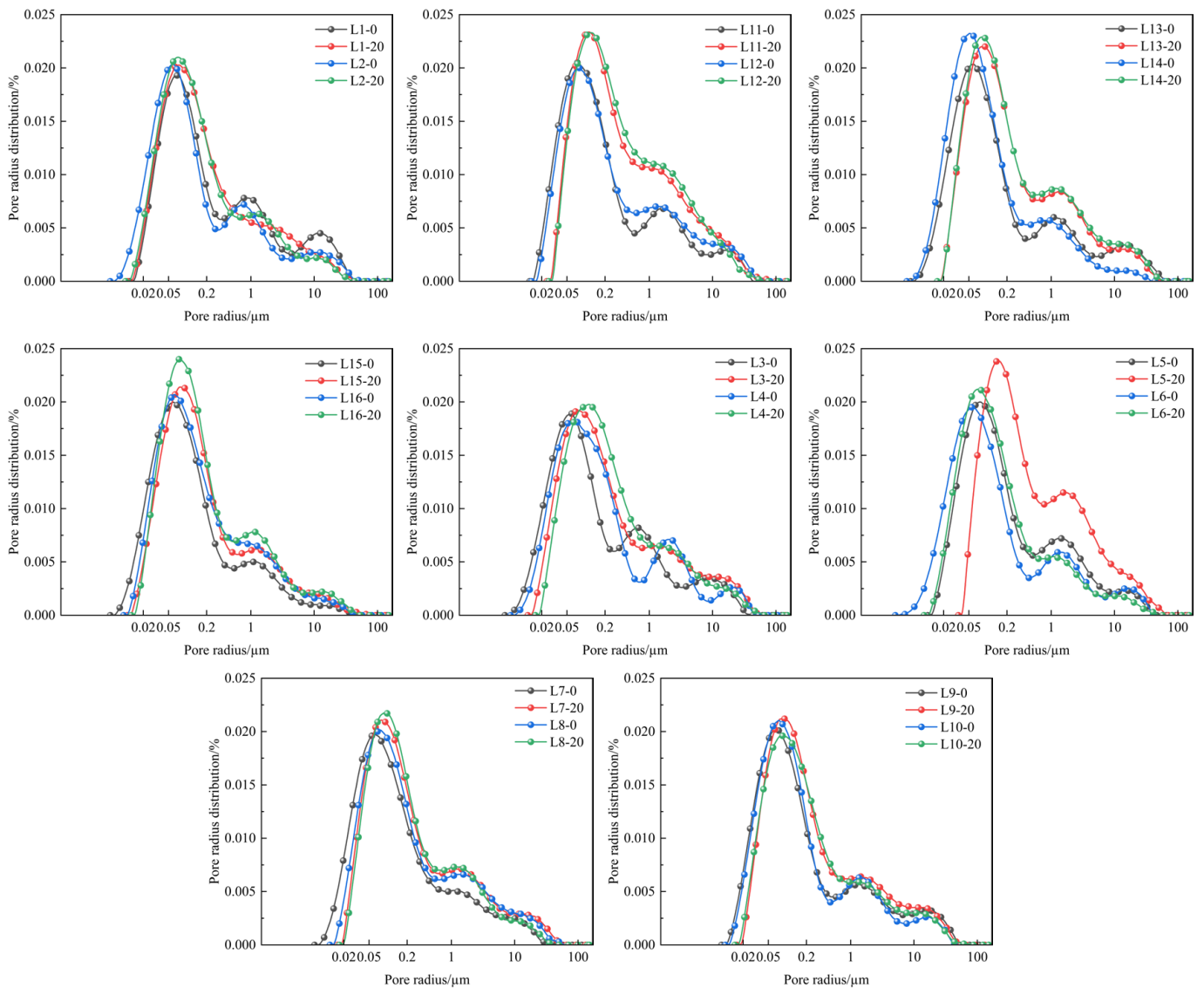


FIGURE 5. Pore radius distribution of CSG before and after freezing–thawing cycles.

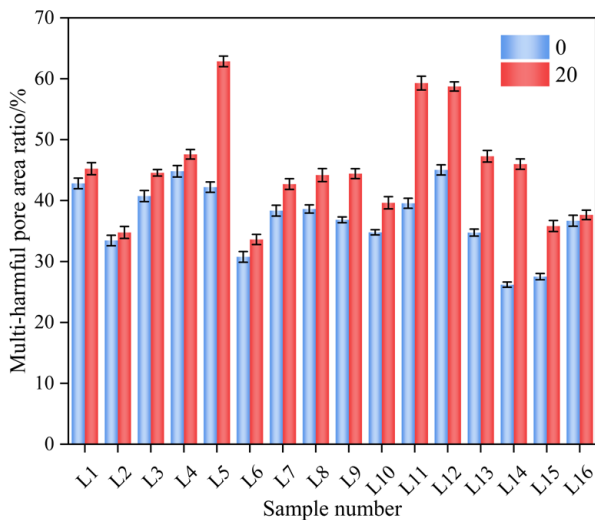


FIGURE 6. Multiple-harmful pore area ratios.

images are shown. Figure 8(a) shows that the microstructure of the blank Group L1 before freezing is needle-shaped, and the surface is flat and has cracks. The energy spectrum analysis reveals that the needle-like substance is ettringite, because it contains Si, Al, Ca and other elements (38, 39). Figure 8(b) shows the morphology of the blank Group L1 after freezing. In the needle-like substance fractures, the pores gradually expand into connected cavities, and the compactness of the test pieces decreases. Since the selected SEM image size is 100 μm , combined with the pore size distribution of NMR, it is considered a more harmful pore. Figure 8(c), (e) and (g) show the pre-freezing microstructures of the L5, L12, and L13 groups, which have obvious changes compared with Figure 8(a). This is because different admixtures have different enhancement mechanisms (40, 41), and they can improve the cementing effect of the gel or the

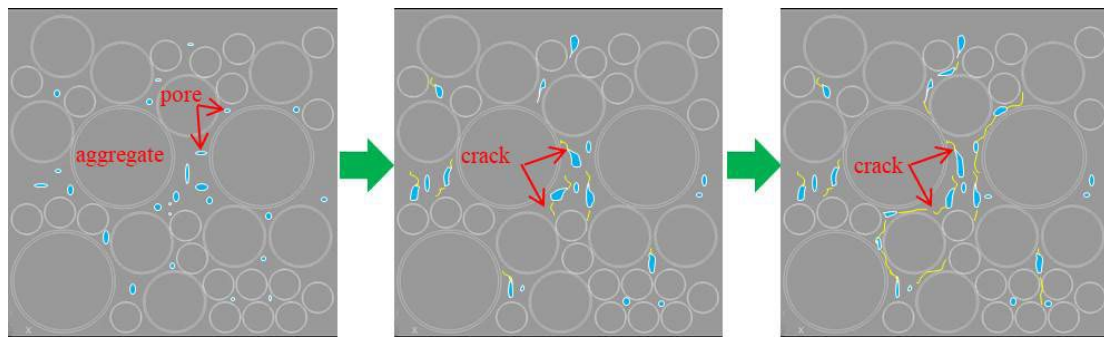


FIGURE 7. Destruction morphology of the pore structure under the action of CSG freeze-thaw cycles.

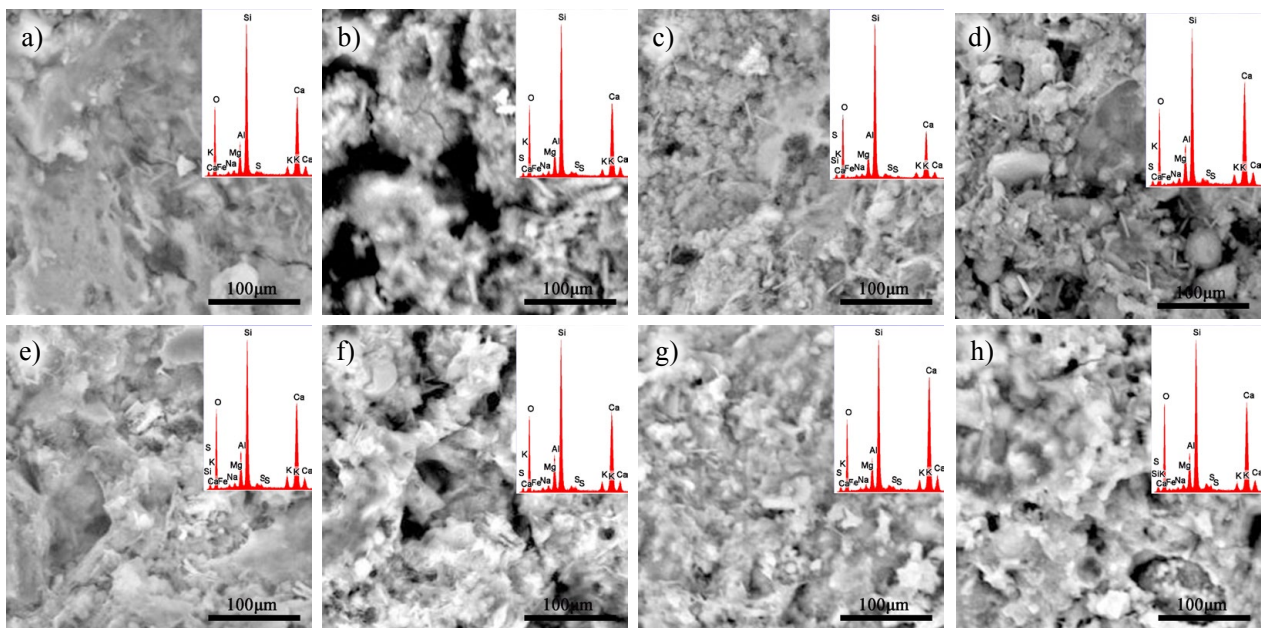


FIGURE 8. SEM images of CSG.

weak area of the aggregate interface to different degrees. After freeze-thaw damage, the deterioration of the pore structure in Figure 8(d), (f) and (h) changes compared with Figure 8(b). The connected pores are significantly reduced and gradually become independent pores with smaller sizes, macroscopically indicating the improvement of the freezing resistance of the test samples. This is the same as the pore size distribution law obtained by NMR experiments.

Through EDS analysis, the hydration products of CSG mainly included C-S-H gel, AFm and AFt. After 20 freeze-thaw cycles, the needle-shaped C-S-H gradually became thicker and even lumpy, resulting in no cross-linking at the terminal, so that the voids could not be filled, and the compactness and freezing resistance were reduced.

To further clarify the changes in the internal pore structure during the freezing and thawing process, we calculated the fractal characteristics of the pore structure on the selected SEM images before and after freezing and thawing using PCAS software. The results are shown in Table 7.

TABLE 7. Fractal dimension of the pore structure of CSG 1000 times SEM images.

Sample number	Fractal dimension before freezing	Fractal dimension after freezing	Change ratio
L1	1.1565	1.1791	1.95%
L2	1.1598	1.1703	0.91%
L3	1.1657	1.1911	2.18%
L4	1.1747	1.1976	1.95%
L5	1.2119	1.2421	2.49%
L6	1.1715	1.1884	1.44%
L7	1.1836	1.2082	2.08%
L8	1.2011	1.2149	1.15%
L9	1.1610	1.1645	0.30%
L10	1.1688	1.1856	1.44%
L11	1.2184	1.2546	2.97%
L12	1.2229	1.2628	3.26%
L13	1.1785	1.2068	2.40%
L14	1.2038	1.2389	2.92%
L15	1.1936	1.2144	1.74%
L16	1.2089	1.2301	1.75%

It can be seen in the table that the fractal dimension of pores improves to varying degrees after 20 freeze–thaw cycles. Among them, the fractal dimension before and after freezing and thawing in the L5, L11, L12, L13, and L14 groups changes more distinctly, which indicates that the pores deteriorate after freezing and thawing. The fractal dimension change rate of the L9 group before and after freezing and thawing was the lowest, at only 0.30%; meanwhile, its compressive strength was also better. Therefore, the fractal dimension of 1000 times SEM images can be used to characterize the freeze–thaw characteristics of CSG.

4. OPTIMAL GROUP VERIFICATION TEST

In summary, the macroscopic mechanical properties of the L9 group are the best, and the strength loss rate after 20 freeze–thaw cycles is only 0.92%. The micropore structure shows that the area occupancy of more harmful pores is the lowest after freezing and thawing. To verify that the composite admixtures in the optimal Group L9 improved the freezing resistance of CSG, further experiments were performed at different water–binder ratios, sand ratios, and cement contents, during which the compressive strength was used as an indicator to evaluate how the admixtures enhanced the freezing resistance of CSG. The mixing ratios and test results are shown in Table 8.

Table 8 shows that the compressive strength of test group L9 mixed with composite admixtures is significantly higher than that of blank group L1, and after 20 freeze–thaw cycles, the compressive strength loss rate ranges within -3.5%~2.7%, which is lower than that (22.5%) of blank group L1 and the effect of a single admixture. Even when the water–binder ratio, sand ratio and cement content are changed, admixtures (containing sodium dodecyl sulfate, graphene oxide, nano silicon powder, and water reducing agent) in the L9 group can significantly enhance the freezing resistance of CSG, Which can improve the service life of the CSG structures in severely cold areas.

5. CONCLUSIONS AND PROSPECTS

In this paper, based on the macroscopic mechanical properties and microscopic pore structure characteristics, the effects of composite admixtures on the freezing resistance durability index strength, relative dynamic elastic modulus, harmful pore occupancy and fractal dimension of CSG were discussed. The following conclusions were drawn:

(1) After 20 freeze–thaw cycles, both the compressive strength and dynamic elastic modulus of CSG decrease. The comparison shows that the strength of L9 (containing sodium dodecyl sulfate, graphene oxide, nano silicon powder, and water reducing agent) meets the design requirements, and its freezing resistance (more than 75% relative to dynamic elastic modulus, lowest strength loss rate) is also good. Such results were confirmed through further experiments, and it was found that under the experimental conditions of different water–binder ratios, sand ratios and cement content, composite admixtures in the L9 group can significantly improve the freezing resistance of CSG.

(2) The NMR test shows that the harmless pores, less harmful pores and harmful pores are mainly in the first peak with a small area occupancy and have little influence on the freezing resistance of CSG with composite admixtures. The area occupancy of more harmful pores (>200 nm) is the main factor affecting the freezing resistance.

(3) Upon analysis of the fractal characteristics of the pore structure of CSG, the fractal dimension increases after 20 freeze–thaw cycles, indicating that the pore structure has deteriorated. Among them, the fractal dimension after freezing in the L9 group is the smallest, signifying that the pore structure of CSG deteriorates less and the freezing resistance remains good.

(4) This article explores the effect of composite admixtures on the freezing resistance of CSG and obtains the optimal composite admixture after comprehensive analysis of various indicators, but it does not studied the enhancement mechanism of a single admixture on the freezing resistance of CSG.

TABLE 8. Validation of mix proportion and compression value of test group.

Sample	Sand rate	Cement /kg/m ³	Fly ash /kg/m ³	Water /kg/m ³	Sand /kg/m ³	Big stones /kg/m ³	Small stones /kg/m ³	Compressive strength/MPa		Loss rate/%
								Before freezing	After freezing	
L1	0.3	70	20	108	630.6	882.84	588.56	10.4	8.06	22.5%
S1	0.3	70	20	108	630.6	882.84	588.56	10.9	10.7	1.8%
S2	0.2	70	20	90	424.0	1017.6	678.4	11.5	11.9	-3.5%
S3	0.2	70	20	108	442.0	996.0	664.0	11.3	11.0	2.7%
S4	0.3	60	20	96	637.2	892.08	594.72	10.7	10.5	1.9%

AUTHOR CONTRIBUTIONS:

Conceptualization: W. Wang. Data curation: L. Zhong. Formal analysis: L. Guo. Funding acquisition: L. Guo. Investigation: W. Wang. Methodology: P. Chen. Project administration: L. Zhong. Resources: M. Wang. Software: Y. Guo. Supervision: L. Guo. Validation: M. Wang. Visualization: L. Wang. Writing, original draft: L. Guo. Writing, review & editing: L. Guo.

ACKNOWLEDGMENTS

This research was funded by National Natural Science Foundation of China: (5210090341) Macro and meso mechanism of damage evolution of cement-sand-gravel dam under extreme temperature and Natural Science Foundation of Henan Province: (202300410270) Research on Frost Resistance Durability Behavior and Deterioration Damage Mechanism of Cemented Sand and Gravel.

REFERENCES

- Omran, M.E.; Tokmechi, Z. (2010) Sensitivity analysis of symmetrical hard fill dams. *Middle East J. Sci. Res.* 6 [3], 251-256.
- Cai, X.; Wu, Y.; Guo, X.; Ming, Y. (2012) Research review of the cement sand and gravel (CSG) dam. *Front. Struct. Civ. Eng.* 6 [1], 19-24. <https://doi.org/10.1007/s11709-012-0145-y>.
- Jia, J.; Lino, M.; Jin, F.; Zheng, C. (2016) The cemented material dam: a new, environmentally friendly type of dam. *Engineer.* 2 [4], 490-497. <https://doi.org/10.1016/J.ENG.2016.04.003>.
- Hirose, T.; Fujisawa, T.; Yoshida, H.; Kawasaki, H.; Hirayama, D.; Sasaki, T. (2018) Concept of CSG and its material properties. In Proceedings of the 4th International symposium on roller compacted concrete dams (pp. 465-473).
- Guo, L.; Li, S.; Zhong, L.; Guo, L.; Wang, L.; Zhang, F.; Zhang, Y.; Wang, M. (2021) A study on the effects of the fractal characteristics of aggregates on the mechanical behavior of cemented sand and gravel. *Mater. Construcc.* 71 [342], e250. <https://doi.org/10.3989/mc.2021.13020>.
- Sanrı-Karapınar, I.; Pehlivan, A.O.; Karakuş, S.; Özsoy-Özbay, A.E.; Yazgan, A.U.; Taşaltın, N.; Kilislioğlu, A. (2020) Application of novel synthesized nanocomposites containing κ-carrageenan/PVA/eggshell in cement mortars. *Mater. Construcc.* 70 [340], e235. <https://doi.org/10.3989/mc.2020.06720>.
- Yildirim, M.; Derun, E.M. (2018) The influence of CuO nanoparticles and boron wastes on the properties of cement mortar. *Mater. Construcc.* 68 [331]. <https://doi.org/10.3989/mc.2018.03617>.
- Hernández, E.F.; Cano-Barrita, P.F.; Torres-Acosta, A.A. (2016) Influence of cactus mucilage and marine brown algae extract on the compressive strength and durability of concrete. *Mater. Construcc.* 66 [321], e074. <https://doi.org/10.3989/mc.2016.07514>.
- Silva, B.; Pinto, A.P.F.; Gomes, A.; Candeias, A. (2021) Admixtures potential role on the improvement of the freeze-thaw resistance of lime mortars. *J. Build. Eng.* 35, 101977. <https://doi.org/10.1016/j.jobte.2020.101977>.
- Behfarnia, K.; Salemi, N. (2013) The effects of nano-silica and nano-alumina on frost resistance of normal concrete. *Constr. Build. Mater.* 48, 580-584. <https://doi.org/10.1016/j.conbuildmat.2013.07.088>.
- Ozgan, E.; Bektas, S. (2011) An investigation of the pull-out strength of asphalt concrete exposed to varying freezing and thawing cycles. *Exp. Techniq.* 35 [4], 44-51. <https://doi.org/10.1111/j.1747-1567.2010.00659.x>.
- Feng, W. (2013) Studies on cemented sand and gravel dam materials and its application. China Institute of Water Resources and Hydropower Research. Beijing, China (2013).
- Li, J.; Kaunda, R.B.; Zhou, K. (2018) Experimental investigations on the effects of ambient freeze-thaw cycling on dynamic properties and rock pore structure deterioration of sandstone. *Cold. Reg. Sci. Technol.* 154, 133-141. <https://doi.org/10.1016/j.coldregions.2018.06.015>.
- Xu, L. (2015) Study on properties of cemented sand and gravel material in cold area. Harbin Institute of Technology. Harbin, China (2015).
- Feng, W.; Jia, J.-S.; Ma, F.-L. (2013) Study on durability of cemented sand gravel dam materials and development of new protective materials. *J. Hydraul. Eng.* 44 [04], 500-504.
- Matsumura, K.; Higuchi, K.; Iwamoto, Y. (2004) Freeze-thaw resistance and use of poor quality construction material. *J. Japan Soc. Eros. Contr. Engineer.* 57 [4], 60-65. <https://doi.org/10.11475/sabo1973.57.4.60>.
- Chen, S.; Zheng, Y. (2018) Study on the evolutionary model and structural simulation of the freeze-thaw damage of cemented sand and gravel (CSG). *J. Inst. Eng. (India) Ser. A.* 99, 699-704. <https://doi.org/10.1007/s40030-018-0319-2>.
- Jin, G.; Kim, K.; Moon, H.; Quan, H. (2016) Long-Term compressive strength and durability properties of "CSG" materials by freezing-thawing test. *J. Korean Geo-Environ. Soc.* 17 [12], 35-43. <https://doi.org/10.14481/jkges.2016.17.12.35>.
- Yeon, K.-S.; Kim, Y.-I.; Hyun, S.-H.; Kim, Y.-S. (2010) Compressive strength properties and freezing and thawing resistance of CSG materials. *J. Korean Soc. Agricul. Engineers.* 52 [1], 51-59. <https://doi.org/10.5389/KSAE.2010.52.1.051>.
- Tanyildizi, H.; Şahin, M. (2015) Application of Taguchi method for optimization of concrete strengthened with polymer after high temperature. *Constr. Build. Mater.* 79, 97-103. <https://doi.org/10.1016/j.conbuildmat.2015.01.039>.
- Sevinc, A.H.; Durgun, M.Y.; Eken, M. (2017) A Taguchi approach for investigating the engineering properties of concretes incorporating barite, colemanite, basaltic pumice and ground blast furnace slag. *Constr. Build. Mater.* 135, 343-351. <https://doi.org/10.1016/j.conbuildmat.2016.12.209>.
- Ministry of Housing and Urban and Rural Construction of the People's Republic of China, GB/T 50081—2019, Standard test method for physical and mechanical properties of concrete (2019), China building industry press, Beijing.
- State Energy Bureau of the People's Republic of China, DL/T 5433-2009, Test specification for hydraulic roller compacted concrete(2009), China building industry press, Beijing.
- Ministry of Housing and Urban and Rural Construction of the People's Republic of China, GB/T 50082-2009, Standard test method for long-term performance and durability of ordinary concrete (2009), China building industry press, Beijing.
- Liu, C.; Shi, B.; Zhou, J.; Tang, C. (2011) Quantification and characterization of microporosity by image processing, geometric measurement and statistical methods: Application on SEM images of clay materials. *Appl. Clay. Sci.* 54 [1], 97-106. <https://doi.org/10.1016/j.clay.2011.07.022>.
- Guo, L.P.; Zhu, Q.; Ling, S. (2019) Study on basic properties and pore characteristics of recycled aggregate pervious concrete. *Water power.* 45 [12], 117-122.
- Du, R.; Zhang, X.; Gu, M.; Ji, T. (2019) The composition effect and mechanism of polycarboxylate superplasticizer and early strength agent. *Mater. Rep.* 33 [14], 2461-2466. <https://doi.org/10.11896/cldb.18040139>
- Ministry of Water Resources of the People's Republic of China. SL678-2014, Technical guidelines for cemented granular materials dam construction (2014), China Water Conservancy and Hydropower Publishing House, Beijing.
- Wang, D.; Zhao, Q.; Yang, C.; Chi, Y.; Qi, W.; Teng, Z. (2020) Study on frost resistance and vegetation performance of seashell waste pervious concrete in cold area. *Constr. Build. Mater.* 265, 120758. <https://doi.org/10.1016/j.conbuildmat.2020.120758>.
- Liu, H.S.; Yang, S.F.; Guo, L.X.; Guo, L. (2019) Freeze-thaw test of gelatinized sand and gravel and analysis of influencing factors. *Water Resour. Power.* 37 [03], 100-102.
- Yun, H.-D.; Rokugo, K. (2012) Freeze-thaw influence on the flexural properties of ductile fiber-reinforced cementitious

- composites (DFRCCs) for durable infrastructures. *Cold. Reg. Sci. Technol.* 78, 82-88. <https://doi.org/10.1016/j.coldregions.2012.02.002>.
32. Zhang, D.; Mao, M.; Zhang, S.; Yang, Q. (2019) Influence of stress damage and high temperature on the freeze-thaw resistance of concrete with fly ash as fine aggregate. *Constr. Build. Mater.* 229, 116845. <https://doi.org/10.1016/j.conbuildmat.2019.116845>.
 33. Zhao, R.; Yuan, Y.; Cheng, Z.; Wen, T.; Li, J.; Li, F.; Ma, Z.J. (2019) Freeze-thaw resistance of Class F fly ash-based geopolymer concrete. *Constr. Build. Mater.* 222, 474-483. <https://doi.org/10.1016/j.conbuildmat.2019.06.166>.
 34. Zhou, C.; Ren, F.; Wang, Z.; Chen, W.; Wang, W. (2017) Why permeability to water is anomalously lower than that to many other fluids for cement-based material? *Cem. Concr. Res.* 100, 373-384. <https://doi.org/10.1016/j.cemconres.2017.08.002>.
 35. Wang, X.; Shen, X.; Wang, H.; Gao, C.; Zhang, T. (2016) Nuclear magnetic resonance analysis of freeze-thaw damage in natural pumice concrete. *Mater. Construcc.* 66 [322], e087. <https://doi.org/10.3989/mc.2016.09014>.
 36. Cano-Barrita, P.F. de J.; Castellanos, F.; Ramírez-Arellanes, S.; Cosmes-López, M.F.; Reyes-Estevez, L.R.; Hernández-Arrazola, S.E.; Ramírez-Ortíz, A.E. (2015) Monitoring compressive strength of concrete by nuclear magnetic resonance, ultrasound, and rebound hammer. *ACI. Mater. J.* 112 [1], 147-154. <https://doi.org/10.14359/51686984>.
 37. Wu, Z.W. (1979) An approach to the recent trends of concrete science and technology. *J. Chinese Ceram. Soc.* [03], 262-270.
 38. Sun, H.R.; Zou, C.X.; Xue, H.J.; Zhao, Q.; Wu, J. (2021) Fractal characteristics of dry-wet and freeze-thaw erosion pore structure of mold-bag concrete. *J. Build. Mater.* 25 [02], 124-130.
 39. Zhou, X.; Hao, X.; Peng, J.; Luo, Z. (2017) Effect of compound admixtures on hydration characteristics of ferrochrome slag based composite material. *Mater. Rep.* 31 [04], 121-125. <https://doi.org/10.11896/j.issn.1005-023X.2017.04.026>.
 40. Ren, X.; Hu, G.H.; Wu, F.; Huang, L. (2019) Effect of nano silica power on mechanical and shrinkage properties of high volume rubber mortar. *Sci. Technol. Engineer.* 19 [22], 299-304.
 41. Zhang, Z.; Wu, J.; Yang, J.; Zhou, J.; Li, D. (2019) Effect of graphene oxide on properties of cement-based self-leveling mortar. *Mater. Rep.* 33 [02], 240-245. <https://doi.org/10.11896/cldb.201902008>